Enhancing Clear-Water General Scour Depth Estimation at Long Channel Contractions: Integrating a Multi-Kernel Relevance Vector Machine Model with a Hybrid Optimization Approach

Elham Ghanbari-Adivi [*,1] , Nariman Mehranfar [2] , Mohammad Khosravi-Hamole [3]

1. Department of Water Engineering, Shahrakord University, Shahrakord, Iran; Associate Professor, Water Research Center, Shahrekord University, Shahrekord, Iran.
2. Department of Civil, Mining and Geology, Faculty of Polytechnique, Montreal University, Quebec, Canada.
3. Department of Water Engineering, Shahrakord University, Shahrakord, Iran.

***Corresponding Author:**
Elham Ghanbari-Adivi

Email: ghanbariadivi@sku.ac.ir
Received: 2026.08.28
Accepted: 2026.10.05
J. Hydraul. Struct., 2027;13(2):15-43
DOI: 10.22055/jhs.2026.52378.1386

ABSTRACT

Scour is a critical phenomenon in hydraulic engineering that can have different consequences for hydraulic structures depending on the depth. Therefore, this study focuses on the accurate estimation of general scour depth at long channel contractions under clear-water flow conditions, which is an important issue in hydraulic engineering. In the first step, a new estimation model called the multi-kernel relevance vector machine model (MKRVM) was developed. The MKRVM model combined sigmoid kernel function (SKF), polynomial kernel function (PKF), and radial basis kernel function (RKF) to improve the performance of the relevance vector machine (RVM) model in estimating scour depth. In the second step, a new optimizer called the genetic algorithm (GA)-Ali Baba forty thieves optimization (AFTOA)-sine cosine optimization (SCO) was developed to fine-tune the MKRVM parameters. Finally, a comprehensive dataset consisting of 140 experimental scour-depth records, compiled from five laboratory studies on clear-water scour at long channel contractions, was used to estimate the scour depth. The GA-AFTOA-SCO-MKRVM model was benchmarked against the GA-AFTOA- SCO-RVM-RKF, GA-AFTOA-RVM- SCO-SKF, GA-AFTOA-RVM- SCO-PKF, GA-AFTOA-SCO- multilayer perceptron (MLP), GA-AFTOA-SCO-radial basis function (RBFNN) model, and empirical models. In addition, the GA-AFTOA-SCO algorithm was compared with several established optimization algorithms. The analysis results showed that the GA-AFTOA-SCO-MKRVM model improved the testing Nash–Sutcliffe Efficiency (NSE) of the other optimized MKRVM models by 6.25-31%. Moreover, the GA-AFTOA-SCO-MKRVM model improved the testing Willmott's index of agreement (WIA) of other estimation models by 8.6-18%. The study also revealed several important findings. First, it was demonstrated that the GA-AFTOA-SCO algorithm achieved better accuracy and faster convergence compared to established algorithms. Second, it was found that incorporating multiple kernel functions enhanced the performance of the RVM model in estimating the scour depth. The results of the study suggest that the GA-AFTOA-SCO-MKRVM model is reliable for estimating scour depth at long channel contractions under clear-water flow conditions.

KEYWORDS

Scour depth, Channel contraction hydraulics, Multi kernel function, Ali Baba forty Thieves optimization, Relevance vector machine model

1. Introduction

Scour is the erosion and removal of bed sediment caused by the erosive action of flowing water, and its accurate estimation is one of the most important design considerations for hydraulic structures such as bridges, weirs, and channel transitions. When a channel narrows at a contraction, the acceleration of flow increases the bed shear stress and produces a localized lowering of the bed, referred to as general scour at the contraction, whose maximum depth governs the structural safety of the transition and of the structures located within it [1]. Reliable indirect estimation of this scour depth is therefore essential for the safe and economical design of hydraulic structures. This article introduces a new hybrid machine-learning-based model for estimating the general scour depth at long channel contractions under clear-water flow conditions.

1.1 Problem statement

Scour refers to the process of erosion or removal of sediment particles from the bed of a channel [2]. It occurs when the velocity of water is high enough to transport and dislodge sediment from the channel bed. Scour has different consequences for the ecosystem and hydraulic structures that vary depending on the depth [3]. While deep scour depths pose a threat to the stability of bridges, dams, coastal structures, and other hydraulic structures, shallow scour depths can lead to the erosion of riverbanks and disrupt the natural habitat of aquatic organisms [4, 5]. Therefore, it is crucial to accurately measure and monitor the depth of scour to ensure the safety and stability of infrastructures and the preservation of ecosystems [6]. Furthermore, measuring scour depth is essential for assessing the effectiveness of erosion control measures and designing resilient infrastructures [7]. The primary focus of this article is to develop a new model for estimating scour depth. Subsequently, the phenomenon of scour in channel contractions is defined, followed by a critical review of the advantages and limitations of existing estimation models.

1.2 Advancements in scour depth estimation: defining, analyzing, and introducing New Models

Scour depth directly affects the stability and safety of various hydraulic structures. This parameter refers to the maximum depth of erosion that occurs in the bed channels and is influenced by factors such as water velocity, turbulence, sediment type and size, and hydraulic conditions [8]. However, accurately measuring scour depth can be challenging due to the dynamic nature of water flow and sediment transport.

The scour depth can be measured using either direct or indirect measurement methods. The direct measurement methods entail the following techniques:

- Sonic Echo Sounder (SES): This non-intrusive method provides real-time data and can penetrate through turbid water. However, it requires calibration and may be influenced by fluctuations in the water column and sediment composition, leading to possible errors [9].
- Divers: Divers can directly observe and measure the depth of scour around underwater structures. However, it is important to note that this method is only effective at shallow depths and clear water.
- Acoustic Doppler Current Profiler (ADCP): This remote sensing technique provides velocity profiles to estimate scour depth indirectly [10]. It is non-intrusive and can cover large areas efficiently. However, ADCP measurements require complex data processing and assumptions about sediment properties, which can introduce uncertainties [10].
- Video-based methods: Video cameras or remotely operated vehicles (ROVs) can be used to record visual observations of the scour area [11]. This method provides visual documentation. However, it is important to note that this method requires clear water conditions and may have limitations in accurately measuring scour

depth.

As mentioned above, various direct measurement techniques have their own advantages and disadvantages. While direct methods such as Sonic Echo Sounder (SES), divers, Acoustic Doppler Current Profiler (ADCP), and video-based methods offer valuable insights into scour depth, they also face challenges such as calibration requirements, and potential errors due to sediment composition or data processing. As a result, researchers have been exploring alternative methods, such as indirect measurement methods, to estimate the scour depth. The indirect measurement methods include numerical models, empirical models, and machine learning models. Numerical models provide detailed insights into the scouring process and can account for complex flow conditions and sediment dynamics [4]. However, they require extensive computational resources and expertise for development and validation. On the other hand, empirical models are easier to use and can quickly estimate scour depth based on available data [12]. However, they may not be as accurate or applicable as numerical models, particularly under unusual or extreme flow conditions. Consequently, machine learning models have gained significant attention from the scientific community for estimating scour depth [4]. These models offer different advantages for analyzing and predicting complex phenomena such as scour depth. One of the key advantages of these models is their ability to handle complex relationships between variables [3]. They can also detect and capture nonlinear relationships, interactions, and dependencies that may exist in the data. Additionally, they are well-suited for handling large and diverse datasets [7]. Due to these advantages, researchers have developed various types of machine learning models for a wide range of applications. Recent studies have continued to advance data-driven scour estimation, for example by coupling gradient-boosting models with metaheuristic hyperparameter optimization for pier scour under clear-water and live-bed conditions [13], and by combining evolutionary symbolic regression with explainable-AI techniques to identify the physical drivers of scour [14]. Among these models, relevance vector machine (RVM) models have shown significant efficacy in various applications particularly in scenarios with limited data [15, 16].

Mathematically, RVM models are formulated as a Bayesian regression problem. They use a sparse Bayesian framework to estimate the posterior distribution of the model parameters, which includes both the regression coefficients and the relevance weights associated with each feature [17]. Furthermore, RVM models offer several advantages over other machine learning models, which are explained as follows:

- Handling Non-Linear Data: RVM can effectively handle non-linearly separable data by using appropriate kernel functions. By mapping the input features into a higher-dimensional space, RVM can discover complex patterns and capture intricate relationships between variables [18]. This flexibility makes RVM suitable for a wide range of classification and prediction tasks, including those with non-linear decision boundaries.
- Interpretability: RVM provides a sparse representation of the model, making it easier to interpret and understand the relationship between input variables and the target variable in the time series [19].
- Bayesian framework: The RVM model employs a Bayesian approach which enables the estimation of uncertainties. By considering the uncertainties in the model parameters, the RVM can provide more reliable predictions and quantify the confidence in those predictions [19].

The mentioned advantages highlight the versatility and robustness of the RVM model, making it a suitable choice for the current study. Moreover, the literature shows that researchers have widely used the RVM model to estimate different hydraulic variables such as streamflow [16], piezometric heads in earth dams [20], sediment load [21], and seepage [22].

However, while the RVM model is suitable for regression tasks, it has certain limitations. Therefore, the following section delves into the limitations of the RVM model and proposes potential solutions to address these challenges.

1.3 Identifying and addressing limitations of the RVM Model for scour depth estimation

As previously discussed, the RVM model has limitations that influence its performance. These challenges are explained as follows:

Single Kernel function: The RVM model comprises several components, and the kernel function is one of its crucial elements. This function transforms the input data into a higher-dimensional space, where the relationships between data points are more easily discernible [23]. By operating in this higher-dimensional feature space, the RVM model can capture relationships in the data that may not be apparent in the original feature space. However, the original RVM model only uses a single kernel function, which may not fully capture the complexity of relationships in datasets [24]. As a result, this can lead to suboptimal model performance and reduced prediction accuracy. However, one approach to overcome this challenge is to simultaneously use multiple kernel functions in the RVM model. Incorporating multiple kernel functions allows the RVM model to effectively capture the diverse and complex relationships within datasets [25]. This concept is consistent with the broader precedent in hydraulic scour research of combining multiple artificial-intelligence models rather than relying on a single model, which has been shown to improve scour-related predictions in other contexts, such as scour dimensions downstream of screens [26] and in the assessment of protective measures against local pier scour using artificial neural network and adaptive neuro-fuzzy inference system models [27]. Thus, based on this concept, this study introduces a novel model called the multi-kernel RVM model. The new model leverages multiple kernel functions to enhance the performance of the RVM model in estimating the scour depth. However, there is still a limitation that will be investigated in the next section.

Adjustment of parameters: The RVM model includes unknown parameters, such as kernel parameters, that significantly impact its performance. However, it is crucial to accurately tune these parameters in order to optimize the performance of the RVM model [25]. In recent years, researchers have developed various optimization algorithms to address this issue. Although these algorithms are capable of effectively optimizing model parameters, they have some limitations. These limitations include slow convergence and the possibility of getting stuck in local optima. Therefore, this study introduces a new optimizer that overcomes these limitations and effectively adjusts the model parameters. The new algorithm enhances search capabilities in the problem space by combining the advantages of two robust optimization algorithms. The new algorithm can not only effectively adjust the RVM parameters, but also has the potential to solve complex problems. Therefore, this paper aims to enhance the RVM model by addressing its two key limitations. The novelties of the current paper are explained in the next subsection.

1.4 Novelty of the paper

The purpose of this paper is to contribute to the indirect measurement of scour depth. The novelty of this paper is threefold and goes beyond a generic combination of existing techniques. First, unlike previous multi-kernel approaches that typically use a fixed or manually assigned weighting between kernels, the MKRVM model developed here integrates the sigmoid, polynomial, and radial basis kernel functions into a single relevance vector machine through a set of weighting coefficients that are themselves treated as unknown parameters and tuned jointly with the kernel parameters by the optimizer, so that the relative contribution of each kernel is learned from the scour data

rather than fixed a priori. Second, the GA-AFTOA-SCO optimizer is a purpose-built three-stage hybrid that targets two specific, previously identified weaknesses of the AFTOA algorithm: immature random initialization, which is addressed by using a GA to generate a mature initial population, and susceptibility to local optima, which is addressed by using SCO to refine the AFTOA's best solution; this specific combination and the order in which the three algorithms are coupled have not been reported in prior scour-estimation studies. Third, to the best of the authors' knowledge, this is the first application of a multi-kernel relevance vector machine to general (contraction) scour at long channel contractions under clear-water conditions, a scour type for which the majority of prior machine-learning studies (which have concentrated instead on local scour at bridge piers and abutments) do not provide directly applicable models. To the best of the authors' knowledge, the resulting model has not been used in any previous research.

2. Materiel and Methods

This section explains the structure of various estimation models and optimization algorithms used to estimate scour depth. First, the theory behind the RVM model is described. Next, the structure of a new optimizer and a new model is described.

2.1 An introduction to the RVM model

The RVM model is a statistical learning algorithm that is commonly used for regression analysis and has found applications in time series forecasting [28]. It uses a technique called relevance vector learning, which is a variant of Bayesian learning. This technique selects a subset of the training data known as relevance vectors and uses them to predict the target variable.
The mathematical framework of the RVM model is based on Bayesian inference and sparse Bayesian learning [25]. It employs a probabilistic approach to model the relationship between the input variables (time series data) and the output variable (predictive values). his relationship is represented by equation 1.

$$z_u = \sum_{u=1}^{N} \mu_u K(in, in_n) + \beta_0 \quad (1)$$

Where z_u : outputs, in, in_n : inputs, μ_u : weight coefficient, and β_0 : bias. The likelihood function is then computed as follows:

$$p(z|\mu,\sigma) = (2\pi\sigma^2)^{\frac{-N}{2}} exp\left(-\frac{\|z-\phi\mu\|^2}{2\sigma^2}\right) \quad (2)$$

Where $p(z|\mu,\sigma)$: likelihood function and σ: standard deviation. In the next step., the posterior distribution is calculated as follows [18]:

$$p(\mu|\alpha) = \prod_{u=0}^{N} N(\mu_u|0,\alpha_u^{-1}) \quad (3)$$

Where α: a hyperparameter vector. Each posterior distribution has a corresponding weight. The weights of the posterior distribution are described as follows:

$$p(\mu|z,\alpha,\sigma^2) = (2\pi\sigma^2)^{\frac{-N+1}{2}}, \left|\xi^{\frac{-1}{2}} exp\left[-\frac{(\mu-\kappa)^T\xi^{-1}(\mu-\kappa)}{2}\right]\right| \quad (4)$$

Where $\xi = (\sigma^{-2}\phi^T\phi A)^{-1}, \kappa = \sigma^{-2}\xi\varphi^T z$, $A = diag(\alpha_0, \alpha_1, \ldots, \alpha_n)$, and ϕ : kernel function. Finally, the marginal likelihood value of the hyperparameters is computed.

$$p(z|\alpha,\sigma^2) = (2\pi)^{\frac{-N}{2}}|\sigma^2 I + \phi A^{-1}\phi^T|. exp\left[\left\{t^T(\sigma^2 I + \phi A^{-1}\phi^T)^{-1}\frac{z}{2}\right\}\right] \quad (5)$$

The original RVM model uses a kernel function that may not fully capture the complexity of the data. Therefore, a new version of the RVM model was developed in this study to overcome the limitations of the original version of the model.

2.2 MKRVM model

The original version of RVM uses only one kernel function, which limits its ability to analyze complex patterns and data

effectively. To address this issue, this study introduces the Multi-Kernel RVM (MKR) model. This new model employs multiple kernel functions to handle various types of data, thereby comprehensively capturing their complexity. Three kernel functions, namely the sigmoid, polynomial, and radial basis kernel functions, were combined because they are mathematically complementary rather than redundant: the radial basis kernel is well suited to capturing smooth, local, non-linear variations in the data, the polynomial kernel captures global polynomial trends and interactions between input variables, and the sigmoid kernel introduces a neural-network-like, saturating non-linearity. Using only one or two of these kernels would omit at least one of these complementary behaviors, while the good performance and stable convergence achieved with these three kernels (Sections 4.2 and 4.4) indicate that this combination already provides a favorable trade-off between representational richness and the number of parameters that must be optimized; a systematic comparison against combinations of additional kernel types was not performed and is identified as a direction for future work. The different kernel functions are defined as follows [29]:
Polynomial kernel function (RVM-PKF)

$$\phi(in, z) = (in^T z + m)^d \quad (6)$$

- Radial basis kernel function (RVM-RKF)

$$\phi(in, z) = exp\left(-\frac{\|in-z\|^2}{2\tau^2}\right) \quad (7)$$

- Sigmoid kernel function (RVM-SKF)

$$\phi(in, z) = tanh(\rho in^T + z) \quad (8)$$

Where ρ: scaling factor and d: order of kernel function, m: kernel function.
Afterward, the following equation is used to merge the kernel functions and integrate them into the RVM model

$$\phi(in, t) = \lambda_1 \phi_{Polynomial} + \lambda_2 \phi_{Radial} + \lambda_3 \phi_{Sigmoid} \quad (9)$$

Where λ_1, λ_2 and λ_3: weight coefficients, $\phi_{Polynomial}$, ϕ_{Radial}, and $\phi_{Sigmoid}$: polynomial kernel function, radial basis kernel function, and $\phi_{Sigmoid}$: sigmoid kernel function. However, the RVM and MKRVM models have adjustable parameters whose values are unknown and need to be optimized. As a result, this study focuses on developing new optimizers to achieve this goal. In the next section, the structure of these optimizers is explained.

2.3 Optimizers

As previously mentioned, multiple optimizers were used in this study to adjust the RVM parameters. In the first step, a new optimization algorithm was created and then its performance was evaluated by comparison with several established and widely used algorithms. This approach enables a thorough evaluation of the effectiveness and efficiency of the novel optimizer developed in this study.

2.3.1 Ali Baba and the Forty Thieves Optimization Algorithm

In recent years, researchers have developed various optimization algorithms to adjust the parameters of machine learning models. Among these developed algorithms, the Ali Baba and Forty Thieves optimization algorithm (AFTOA) has demonstrated remarkable capability in solving complex problems. Numerous studies have demonstrated its high effectiveness in various fields, such as feature selection [30], training deep learning models [31], optimal power management [32], and data classification [33]. Moreover, the literature review revealed that AFTOA outperformed various optimization algorithms such as the bat algorithm, the genetic algorithm, and the whale algorithm. Therefore, AFTOA is a suitable tool for adjusting the parameters of the machine learning models developed in the current study [30]. The algorithm drew inspiration from the tale of Ali Baba and the Forty Thieves. In the story, a band of forty thieves tried to find Ali Baba after he discovered the location of their treasure and

stole it. Ali Baba had a clever servant named Marjane, who helped him devise clever plans to evade the thieves. In general, the algorithm is based on the behavior of the thieves, Alibaba and Marjaneh during their interactions in the story. The optimization process starts by initializing the thieves' position in the problem space using the following equation [30].

$$th^i = lo_j + ra \times (up_j - lo_j) \quad (10)$$

Where th^i: the location of the ith thief (a candidate solution), lo_j : lower bound of decision variables, up_j : upper bound of decision variables, and ra: random value. The algorithm assumes that the location of Ali Baba represents the optimal solution within the search space. Additionally, the algorithm updates initial solutions based on three different scenarios, which are explained as follows:

- First scenario: The thieves track down Ali Baba and update their position using information acquired from an informant. This behavior is simulated by the following 11 [30]:

$$\begin{aligned} th_{t+1}^i &= g_{est(t)} + [TD_t(best_t^i - o_t^i)r_1 + TD_t(o_t^i - m_t^i)r_2]\, sgn(rand - 0.5) \\ r_3 &\geq 0.5 \\ r_4 &> Pp_t \end{aligned} \quad (11)$$

Where $rand$: a uniform random number that lies in the range (0.5, 1)th_{t+1}^i: the position of thief i at iteration t+1, $g_{est(t)}$: the global best solution, $best_t^i$: the local best solution, TD_t: the tracking distance of the thieves at iteration,Pp_t: the realization potential of the thieves, r_1, r_2, r_3, and r_4: random numbers, o_t^i: the position of Ali Baba at iteration t, rand: random number, m_t^i: Marjaneh's intelligence level, and sgn: it changes the direction of the search

Process. The parameter α is calculated as follows:

$$\alpha = [(n-1).rand(n,1)] \quad (12)$$

Where n: population size, $rand(n,1)$: random number. When the thieves achieve a better location than the previous one, Marjenh changes her tactics for deceiving them. This behavior is simulated by Equation 13 [30]:

$$\begin{aligned} &m_t^{\alpha(i)} = \\ &\begin{bmatrix} th_t^i \leftarrow if\left(f(th_t^i) \geq f(m_t^{\alpha(i)})\right) \\ m_t^{\alpha(i)} \leftarrow \left(f(th_t^i) < f(m_t^{\alpha(i)})\right) \end{bmatrix} \end{aligned} \quad (13)$$

Where: $f(th_t^i)$: The fitness function of the thieves.

- Second scenario: Ali Baba tries to deceive the thieves, but they are aware of his decision and randomly search to find him. This behavior is simulated by using equation 14.

$$\begin{aligned} th_{t+1}^i &= TD_t + [TD_t(up_j - lo_j) + lo_j] \\ r_3 &\geq 0.5 \\ r_4 &\leq Pp_t \end{aligned} \quad (14)$$

- Third Scenario: If the thieves in the first and second scenarios cannot reach the desired location, they update their current location using Equation 15.

$$\begin{aligned} th_{t+1}^i &= g_{est(t)} - [TD_t(best_t^i - o_t^i)r_1 + TD_t(o_t^i - m_t^i)r_2]\, sgn(rand - 0.5) \\ r_3 &< 0.50 \end{aligned} \quad (15)$$

Similar to other algorithms, the AFTOA begins the optimization process by utilizing random solutions. However, this approach can result in slow convergence. In addition, the algorithm can fall into a local optimum due to its reliance on random initializations of solutions for the optimization process. Therefore, these two issues are addressed in the next section.

2.3.2 Genetic algorithm-AFTOA-Sine cosine optimization algorithm

The previous section explained two major issues related to the AFTOA. This section focuses on addressing both of these

problems. First, it is important to note that the initial solutions used by the AFTOA at the beginning of the optimization process are immature. These immature solutions may not accurately represent the problem space and may result in slow convergence as the algorithm refines them iteratively. Thus, it is essential to explore methods for generating more effective initial solutions. One approach is to use another optimization algorithm or metaheuristic to generate initial solutions for the AFTOA. This algorithm should also not be overly complex to ensure that the process remains efficient and practical. Furthermore, the algorithm should be able to explore the problem space efficiently to generate high-quality initial solutions. Among different optimization algorithms, genetic algorithm (GA) can be a suitable choice due to its simplicity and ease of implementation. Furthermore, the literature shows that GA has been successful in various applications such as the optimal power flow problem [34], data sciences [35], image reconstruction [36], and training parameters of prediction models. Therefore, a genetic algorithm is first utilized to solve the optimization problem and generate mature solutions. These solutions are then used as initial solutions for the AFTOA to improve its performance.

However, while the first problem has been addressed, the second problem still remains a challenge. The second issue is that the AFTOA may fall into local optima. One approach to address this problem is to update the last step of the AFTOA algorithm to incorporate mechanisms for escaping local optima. This can be achieved by using another optimization algorithm. The role of this new algorithm is to update the best solution obtained from the GA-AFTOA method. The purpose of this additional optimization step is to improve the quality of the solutions generated by the GA-AFTOA and guide the AFTOA toward more promising areas in the search space. However, there are various optimization algorithms suitable for achieving this objective. In this study, the sine cosine optimization (SCO) algorithm was specifically chosen for three reasons. First, the SCO algorithm utilizes only two equations to update solutions, making it a simple algorithm to implement [37]. Second, compared to other algorithms, the SCO algorithm has fewer parameters, which simplifies the optimization process [38]. Third, this simplicity was validated empirically rather than assumed: SCO was benchmarked against PSO and FOA in the same refinement role within the hybrid framework (Section 4.2), and it consistently produced a lower RMSE and faster convergence (Section 4.2, Figure 5). It is also worth emphasizing that SCO refines the numerical hyperparameters of the MKRVM model (the kernel and weight-coefficient parameters in Equations 6-9), not the physical input variables of the scour-depth relationship; consequently, the number of physical input parameters used to describe the scour process (Equation 27) does not affect the applicability or computational simplicity of SCO. The SCO uses sine and concise functions for updating solutions in the search space [39]. The mathematical model for the SCO is represented by the following equation:

$$S_i^{t+1} = \begin{bmatrix} S_i^{t+1} + ra_1 \times sin(ra_2) \times \left| ra_3 D_i^t - S_i^t \right| \leftarrow ra_4 < 0.50 \\ S_i^{t+1} + ra_1 \times cos(ra_2) \times \left| ra_3 D_i^t - S_i^t \right| \leftarrow ra_4 \geq 0.50 \end{bmatrix} \quad (16)$$

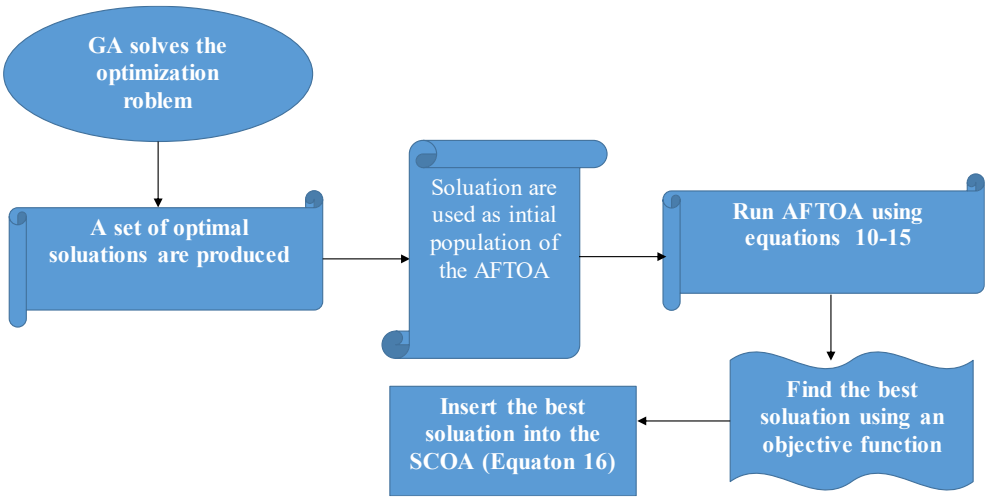


Figure 1. Structure of hybrid algorithm

Where S_i^{t+1}: the location of a new solution at t+1 th iteration, ra_1, ra_2, ra_3, and r_4: random numbers, D_i^t : the location of destination point in ith dimension at t th iteration, and S_i^t: the location of the current solution. The parameter ra_1 is updated as follows:

$$ra_1 = \alpha - t\frac{\alpha}{T} \quad (17)$$

Where t: The number of current iteration, T: The maximum number of iterations. However, the hybrid algorithm is created as follows:

- In the first step, the genetic algorithm is used to solve the given optimization problem. In a genetic algorithm, a population of potential solutions is randomly generated. The algorithm then applies various genetic operators, including selection, crossover, and mutation, to the population. The selection involves selecting individuals from the population to serve as parents for the next generation. Crossover combines the genetic material of two selected individuals to create new offspring [40]. Mutation randomly alters the genetic information of individuals to maintain diversity in the population. The optimization process is repeated for multiple generations, allowing the population to evolve over time. The algorithm iteratively improves the quality of the solutions until a termination condition is met. This condition can be either the attainment of a maximum number of iterations or the achievement of a desired level of solution quality. Then, the generated solutions are used as the initial population of the AFTOA.
- In this step, the AFOTA algorithm is used to find the optimal solutions. The current best solution is then refined and updated using the SCA algorithm. The best solution is inserted into equation 13 as the destination point, which helps generate new solutions. The process continues until the stop conation is met. Figure 1 depicts the structure of the hybrid algorithm.

2.4 Hybrid GA-AFTOA-MKRVM model

In this study, the GA-AFTOA-MKRVM model was utilized to estimate the depth of the scour. To create the new model, the following steps should be followed.

- First, a comprehensive dataset was gathered from multiple sources, including various literature. The details and explanations of this dataset can be found in Section 3.
- The MKRVM parameters include kernel parameters, α , and σ^2 that should be optimized. These parameters are defined as the initial population of the GA. Then, they are inserted into the MRVM model to estimate the scour depth. An objective function such as root mean square error is

used to evaluate the accuracy of the model and determine the quality of the parameters. Finally, the operators of GA are applied to update model parameters and generate a new set of model parameters.

- The new set of model parameters serves as the initial population for the AFTOA and is updated using equations 10-15. Then, the updated parameters are used to run the MKRVM model and calculate the objective function. The objective function helps determine the best solution, which includes a set of parameters that yield the lowest RMSE for the MKRVM model.
- Finally, the current best solution is inserted into equation 16 to produce a new set of parameters. If the desired level of accuracy is achieved, the optimization process will terminate. Otherwise, the MKRVM model goes back to the previous level.

However, it is crucial to address the issue of overfitting when developing the GA-AFTOA-MKRVM model. Overfitting occurs when a model trains well on the training data but does not perform well on unseen data. One effective approach to address this problem is to use K-fold cross-validation. This technique allows the model to learn from different parts of the data, mitigating the risk of overfitting to a particular subset.

The K-fold cross-validation method involves partitioning the dataset into K subsets or folds, where one fold is used as the validation set while the remaining folds are used for training. With the selected value of K=10 (Section 4.1), this corresponds to a 90%/10% training/testing split of the 140-point dataset in each of the 10 iterations, i.e., 126 records for training and 14 records for testing per fold, with every record used exactly once for testing across the 10 folds. The training folds are utilized to train the GA-AFTOA models, while the testing fold is used to evaluate its performance. This process is repeated K times, and the average value of the performance metric is calculated to estimate the overall performance of the model. Several error indices are used in this study to evaluate the performance of the new model and compare it with other existing models [41]. Specifically, RMSE and the coefficient of determination (R^2) are used to quantify overall estimation error and linear agreement, respectively (Sections 4.1, 4.2, and 4.6), NSE and WI are used as normalized, scale-independent measures of model efficiency and agreement (Sections 4.4 and throughout), MAE is used for the heatmap-based model comparisons (Section 4.6), and PBIAS is used to detect systematic over- or under-estimation (Section 4.5); these indices are explained below and, together, provide a more complete assessment of accuracy than any single metric could on its own.

- Root mean square error (RMSE): RMSE is a widely used metric for evaluating the performance of an estimation model. A lower RMSE indicates better accuracy of the estimation model.

$$RMSE = \sqrt{\frac{1}{N}\sum_{i=1}^{N}\left(sd_i^{ob} - sd_i^{es}\right)^2} \quad (18)$$

- Mean absolute error (MAE): MAE is another widely used metric for evaluating the performance of estimation models. Lower MAE values indicate better accuracy.

$$MAE = \frac{1}{N}\sum_{i=1}^{N}\left|\left(sd_i^{es} - sd_i^{ob}\right)\right| \quad (19)$$

- Nash–Sutcliffe Efficiency: The NSE is a statistical measure of model performance commonly used in modeling. The NSE ranges from negative infinity to 1. A value of 1 indicates perfect agreement between the observed and estimated values.

$$NSE = 1 - \left[\frac{\sum_{i=1}^{N}\left(sd_i^{ob} - sd_i^{es}\right)^2}{\sum_{i=1}^{N}\left(sd_i^{ob} - s\bar{d}^{ob}\right)}\right] \quad (20)$$

- Willmott's Index of Agreement (WI): WI assesses the agreement between observed and modeled values. It varies from negative infinity to 1. A value of 1 indicates perfect agreement between measured and estimated values.

$$WI = 1 - \frac{\sum_{i=1}^{N}(sd_i^{ob} - sd_i^{es})^2}{\sum(|sd_i^{ob} - s\bar{d}^{ob}| + |sd_i^{es} - s\bar{d}^{ob}|)} \quad (21)$$

Percentage of bias (PBIAS): PBIAS provides a relative measure of bias. A PBIAS of 0 indicates the highest level of accuracy.

$$PBIAS = \frac{\sum_{i=1}^{n}(sd_i^{ob} - sd_i^{es})}{\sum_{i=1}^{n}(sd_i^{ob})} \quad (22)$$

Where $s\bar{d}^{ob}$: Average observed data, sd_i^{es}: Estimated data, and sd_i^{ob}: Observed data.

2.5 Algorithms and models for comparison

In this study, the MKRVM and AFTOA are used as a new estimation model and optimization algorithm. However, it is necessary to evaluate their performance by comparing them with existing models and algorithms. This comparison provides a better understanding of the advantages and drawbacks of MKRVM and AFTOA in different scenarios and applications. To achieve this, several well-known models and algorithms are utilized, including the multilayer perceptron (MLP) model and radial basis function neural network (RBFNN) for estimation, as well as the firefly optimization algorithm (FOA) and particle swarm optimization (PSO) for optimization. These models and algorithms are explained in the following subsections.

2.5.1 MLP model

The MLP model is a type of artificial neural network that consists of multiple layers of interconnected nodes. The structure of an MLP typically includes an input layer, one or more hidden layers, and an output layer [42]. The input layer is responsible for receiving the input features and transmitting them to the hidden layers. In the hidden layers, each neuron performs a mathematical operation on the received inputs and generates an output [43]. The output layer receives the outputs of the final hidden layer and produces the final prediction or classification results.

2.5.2 RBFNN model

The RBFNN is a type of artificial neural network that is widely used in estimating target variables [44]. It consists of three main layers: the input layer, the hidden layer, and the output layer. The input layer is responsible for receiving input data, which can be features or variables related to the problem being addressed. The hidden layer in the RBFNN model is responsible for transforming the input data into a higher-dimensional feature space. This transformation is achieved using radial basis functions. Specifically, the RBFNN model employs a Gaussian function as the radial basis function in this layer [45]. This Gaussian function calculates the similarity between the input data points and a set of prototypes or center points. Finally, the output layer of the RBFNN model combines the outputs of the hidden units to produce the final prediction or classification. This layer typically uses a linear combination of the output of the hidden units, weighted by coefficients.

2.5.3 PSO algorithm

The PSO algorithm was inspired by the cooperative behavior observed in schools of fish or flocks of birds, which is a characteristic of swarm intelligence algorithms [46]. In this algorithm, particles share their best-found information to collectively search for solutions. Each particle consists of two components: velocity and location. These components are updated using the following equations.

$$v_i^{t+1} = wv_i^t + \xi_1 rand(pe_i - x_i^t) + \xi_2 rand(ge_i - x_i^t) \quad (23)$$

$$x_i^{t+1} = x_i^t + v_i^{t+1} \quad (24)$$

Where v_i^{t+1}: the velocity of the ith particle, ξ_1 and ξ_2 : acceleration coefficient, rand: random number, pe_i: the local best position, and ge_i: the global best location, x_i^{t+1}: new location of particles.

2.5.4 FOA method

The FOA is a nature-inspired optimization algorithm that is based on the flashing behavior of fireflies [47]. Fireflies emit light signals to communicate and the FOA simulates this behavior through a mathematical model. First, the locations of the fireflies are randomly initialized and their fitness is determined by a fitness function [48]. The firefly with the highest fitness is identified as the best firefly, and the locations of the other fireflies are updated using specific equations. Finally, when the stop condition is met, the process ends.

$$F_j(t+1) = F_j(t) + \delta_1 * \left(F_i(t) - F_j(t)\right) + \alpha_1(t) * h * \left(\varepsilon_j - 0.50\right) \quad (25)$$

$$\delta_1 = \delta\left(\delta min_{max} e^{-\gamma r_{ij}^2}\right)_{min} \quad (26)$$

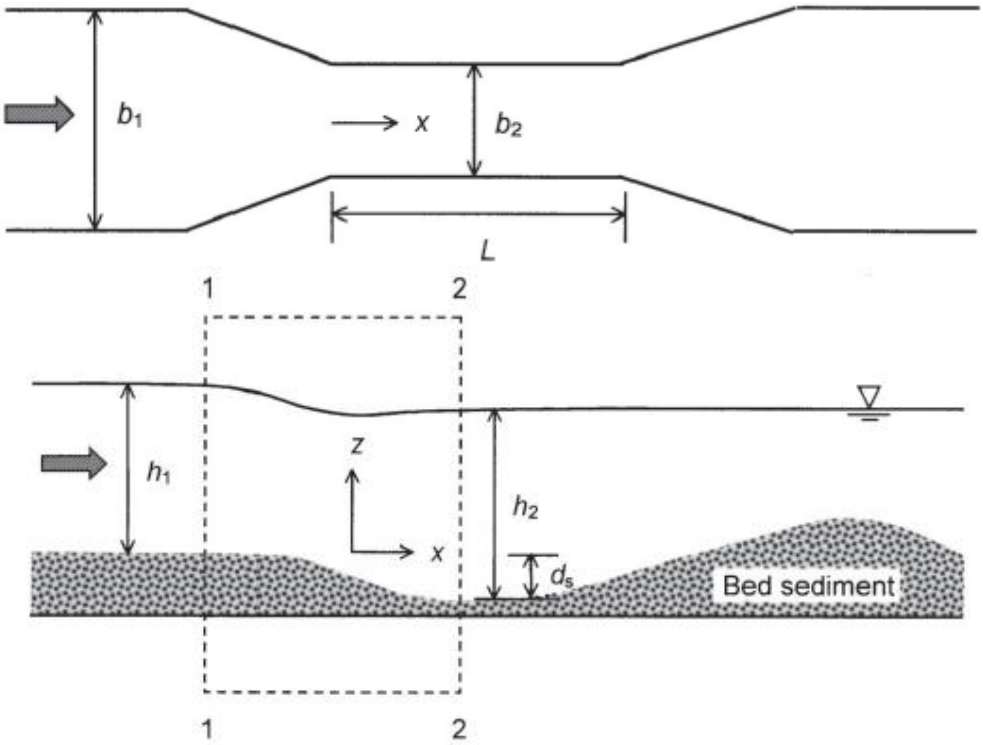
Where $F_j(t+1)$: The location of jth firefly at t+1, $F_j(t)$: The location of the jth firefly at t+1 , $F_i(t)$: The location of the ith firefly, δ_1: The attractiveness, δ_{max} : The maximum attractiveness, $\alpha_1(t)$: a step and δ_{min}: The minimum attractiveness, h: The length scale of the designed variables γ: The coefficient of light absorption, and r_{ij}: the distance between fireflies i and j.

3. Case study

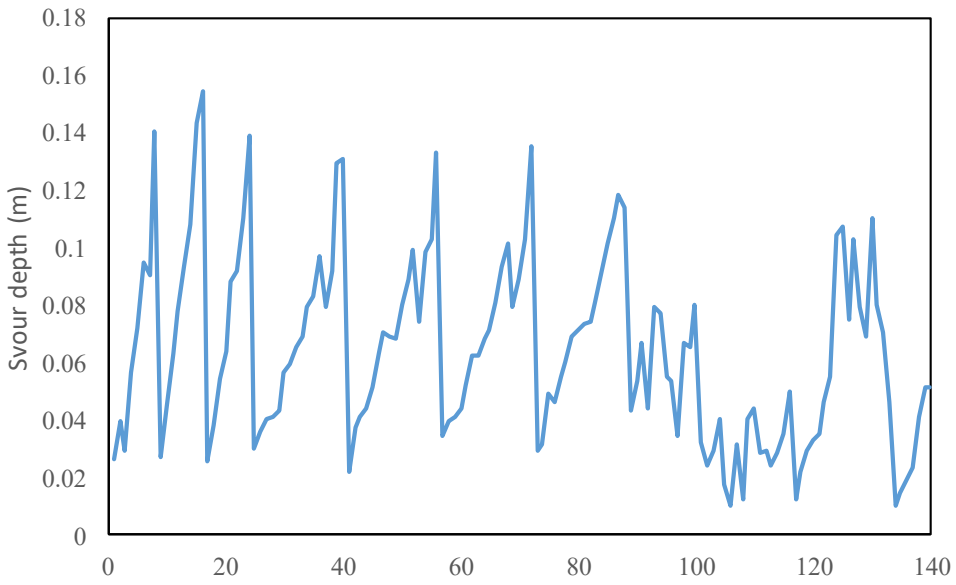
In this study, the GA-AFTOA-MKRVM model was developed to estimate the depth of scour in a channel contraction. Figure 2a depicts the schematic of a long rectangular channel contraction at the equilibrium scour condition. When the channel narrows, the flow area decreases, and the flow velocity increases according to the principle of conservation of mass. This increase in velocity results in higher shear stresses along the channel bed and banks. As a result, sediment particles are mobilized and transported downstream, leading to the formation of the scour hole. Overall, scour formation at the contraction of a channel is a complex phenomenon that is influenced by various factors such as sediment properties, flow conditions, the geometry of the contraction, and environmental conditions. This scour is classified as general (contraction) scour, as distinct from local scour around piers or abutments, because it develops uniformly across the contracted cross-section rather than being concentrated around an isolated obstruction. In this study, all the compiled data correspond to clear-water conditions, in which the approach velocity remains below the critical velocity for sediment entrainment (u1/uc < 1) upstream of the contraction, so that scour at the contracted section develops without a compensating supply of sediment from upstream and progresses until the local shear stress at the contracted section falls to the critical value, at which point the equilibrium scour depth is reached. Numerous studies have identified a governing equation that relates the scour depth to the effective parameters. This relationship is illustrated by Equation 27 [49, 50] (Dey and Raikar, 2005).

$$ds = f\left(\frac{d50}{h1}, \frac{u1}{uc}, \frac{b2}{b1}\right) \quad (27)$$

Where U_1: approaching flow velocity, U_{1ec}: Critical velocity, d_s: Scour depth, h_1 and b_1: geometry of the un-contracted section, b_2: width of the contracted zone. The terms on the left side of Equation 27 are used as inputs to estimate the scour depth. To train and test the models, 140 experimental data points were used. The data were collected from five laboratory studies on clear-water scour at long channel contractions: Dey and Raikar [50], Komura [51], Gill [52], Webby [53], and Lim et al. [54]. The details of the data, including the number of records and the range of each input parameter contributed by each source, are listed in Table 1. Additionally, Figure 2b illustrates the data on scour depth.



(a) (Dey and Raikar, 2005) [50]



(b)

Figure 2. a: schematic of a long rectangular channel contraction at the equilibrium scour condition. and b: data on scour depth

Table 1. Details of used data

Source	No. of Records	d50 (mm)	b2/b1	h1 (m)	u1/uc	Scour depth (m)
Dey and Raikar (2005) [50]	95	0.81 – 14.25	0.40 – 0.70	0.067 – 0.137	0.900 – 0.976	0.022 – 0.154
Komura (1966) [51]	12	0.35 – 0.55	0.25 – 0.50	0.028 – 0.082	0.752 – 1.00	0.034 – 0.080
Gill (1981) [52]	11	0.92 – 1.53	0.66	0.027 – 0.083	0.628 – 0.967	0.010 – 0.050
Webby (1984) [53]	12	2.15	0.33	0.088 – 0.131	0.392 – 0.705	0.055 – 0.117
Lim (1993) [54]	10	0.47	0.30 – 0.65	0.024 – 0.028	0.960 – 1.00	0.010 – 0.051
Total / Global Range	140	0.35 – 14.25	0.25 – 0.70	0.024 – 0.137	0.392 – 1.00	0.010 – 0.154

4. Results and Discussion

4.1 Determination of the number of folds

In the first step, it is important to determine the number of folds in the K-fold cross-validation method. The selection of the number of folds, denoted by 'K', depends on various factors such as the size of the data set, computational resources, and the desired trade-off between bias and variance in model evaluation. Typically, common values for 'K' range from 2 to 10, with K=5 and K=10 being the most frequently recommended in the literature [55]. However, it is crucial to strike a balance between the availability of sufficient data in each fold for reliable evaluation and the efficient use of computational resources. An investigation was conducted to evaluate the impact of different K values (specifically K=2, K=5, and K=10) on the accuracy of the GA-AFTOA-SCO-MKRVM (GASM) model. The GASM model was run with each K value and the corresponding RMSE values were calculated for the same, fixed train-test partition of the data so that the comparison isolates the effect of the fold count rather than of a different data split; these values are presented in Figure 3. Based on the figure, it is clear that the value of K=10 resulted in lower RMSE compared to other values of K. Therefore, K=10 was selected as the optimal value and used for the subsequent modeling reported in this paper. In each fold, the model was optimized using only the training folds, and the RMSE reported for that fold was computed exclusively on the held-out validation fold, which was not used in parameter tuning; the RMSE values in Figure 3 and all subsequent training/testing metrics reported in this study are therefore averages of these out-of-fold values across the K folds, so no data leakage between training and testing occurs at any value of K.

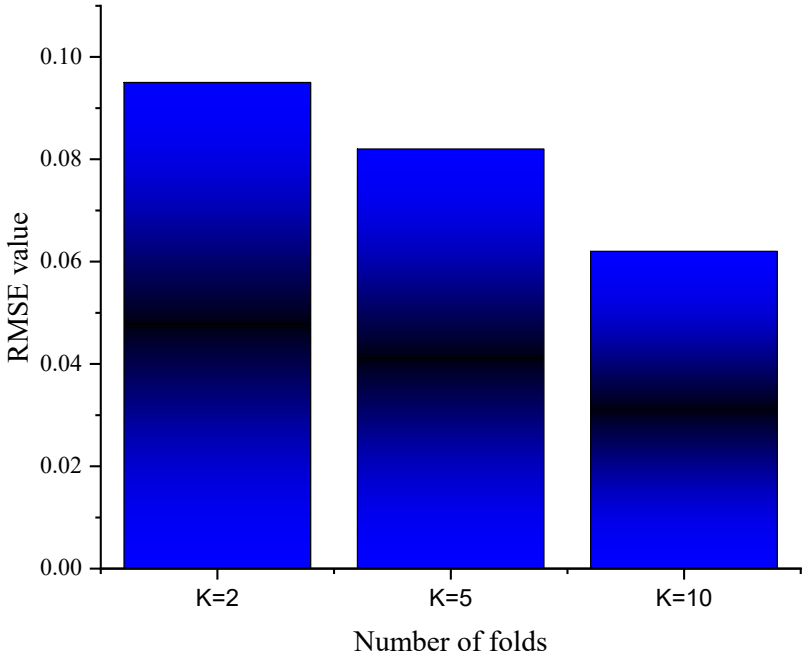


Figure 3. Determination of the optimal value of K

4.2 Determination of the algorithm parameters

In this study, the GA-AFTOA-SCO algorithm was utilized to adjust the model parameters. First, it is necessary to determine the random parameters of the algorithm. The population size is a crucial random parameter. Figure 4 illustrates the impact of this parameter on the RMSE values of the GA-AFTOA-SCO-MKRVM model. The population size for GA ranged from 50 to 300. The lowest RMSE was achieved when the population size was set to 150. Similarly, the population size for AFTOA and SCO also varied from 50 to 300. The lowest RMSE values were obtained when the population sizes were 150 and 200, respectively. Furthermore, Table 2a provides the optimal values for other algorithm parameters. Similarly, these parameter values were obtained using a sensitivity analysis. Table 2b also displays the optimal values for model parameters. The non-monotonic trend in Figure 4, in which RMSE first decreases and then increases with population size, reflects a well-known exploration-exploitation trade-off in population-based metaheuristics: a population that is too small provides insufficient diversity to explore the search space, so the algorithm tends to converge prematurely to a local optimum, whereas an excessively large population increases the diversity of candidate solutions beyond what is needed, so that, for a fixed number of iterations, each individual solution receives fewer effective refinement steps and the search does not fully converge; both regimes therefore result in a higher RMSE than the intermediate, optimal population size.

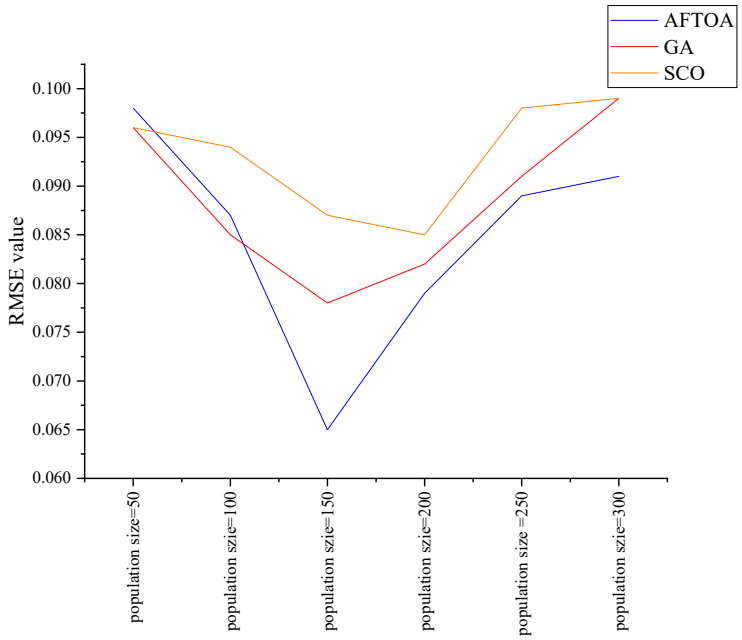


Figure 4. A sensitivity analysis for the determination of the population size

Table 2. a: The optimal values of model parameters, b: The optimal values of model parameters

a

SCO	ra_2=2π/3, $ra_3 = 0.8$, and $ra_4 = 0.2$
GA	Mutation probability: 0.01, Crossover rate=0.9, selection rate=0.40
PSO	w =0.70 and ξ_1=2 and $\xi_2 = 2$
FOA	initial attractiveness=0.20 , The coefficient of light absorption=0.20

b

RVM-PKF	**m=0 and d=2**
RVM-RKF	τ =2
RVM-SKF	ρ =0.10 and z=0
MLP	Number of hidden layers=1 and number of hidden neurons=5
RBFNN	Number of hidden layers=1 and number of hidden neurons=7

After adjusting the algorithm parameters, the models are executed to estimate the scour depth. However, one of the objectives of this paper is to develop a robust algorithm that overcomes two limitations of the AFTOA. Therefore, it is essential to assess the convergence speed of optimizers. Figure 5 illustrates the convergence speed of optimizers. As observed from the figure, the GA-AFTOA-SCO reached convergence earlier than the other optimizers. It achieved convergence after 300 iterations, while the AFTO, SCO, PSO, FOA, and GA achieved convergence after 400, 500, 600, 600, and 700 iterations, respectively. These results highlighted the effectiveness of using GA and SCO in improving the convergence speed of the AFTOA. This improved convergence speed can significantly reduce the computational time required for optimization tasks, making the new algorithm more practical for real-world applications. The findings presented in Figure 5 also provide valuable insights into the performance of different optimization algorithms and underscore the importance of developing robust and efficient optimization techniques.

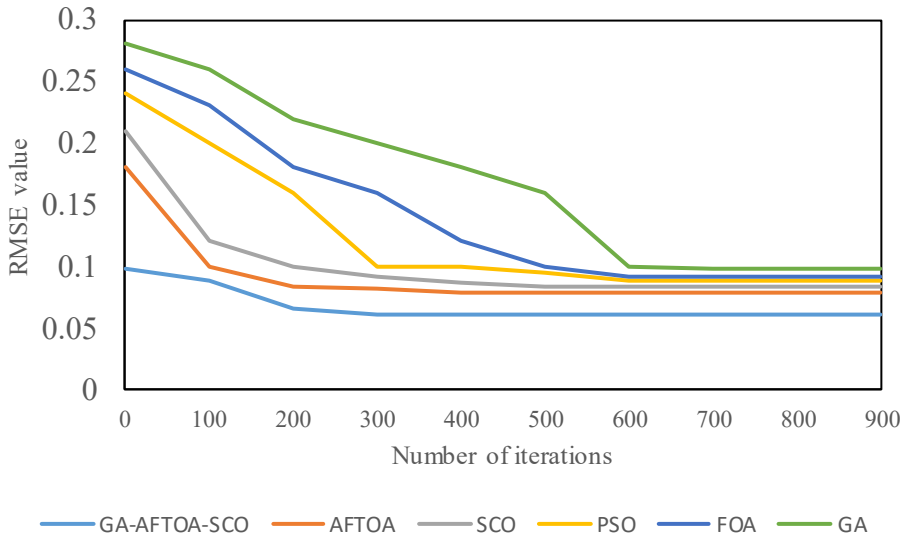


Figure 5. Convergence curve of different optimizers

4.3 Determination of the effect of input parameters on the accuracy of the GA-AFTOA-MKRVM

In this study, the scour depth was estimated using four inputs. However, it was crucial to examine how different parameters influenced the accuracy of the GA-AFTOA-MKRVM model. To investigate this, a sensitivity analysis was conducted. During this analysis, the input parameters were systematically eliminated one by one in order to observe their impact on the model's performance metrics. Table 3 presents the RMSE values for various input combinations. The findings indicated the elimination of $\frac{U_1}{U_c}$ from the initial input combination resulted in an 81% increase in RMSE. This suggested that $\frac{U_1}{U_c}$had the most significant impact on the accuracy of the new model and was therefore the most important input parameter. On the other hand, removing $\frac{b_2}{b_1}$ from the initial input combination only led to a 5% increase in RMSE. This indicated that $\frac{b_2}{b_1}$had the least impact on the accuracy of the GA-AFTOA model.

The results obtained were also consistent with the scour mechanism and could be better understood by examining the fundamental principles of sediment transport and the scour process. When the flow velocity in the channel bed exceeds a critical threshold, the shear stress becomes strong enough to erode the material on the bed. The ratio of flow velocity to critical velocity (u1/uc) directly controls the intensity of the sediment-transporting shear stress relative to the threshold of motion, so that even a moderate change in this ratio produces a disproportionately large change in the equilibrium scour depth; this is why removing it from the input combination produced the largest (81%) increase in RMSE, and it is consistent with its role as the primary driving variable in the governing scour relationship in Equation 27 and in previous long-contraction scour studies [50, 51]. Furthermore, although the ratio of the channel width at contraction to the width of the channel before contraction (b2/b1) is an important factor in determining scour depth because it controls the degree of flow concentration and the resulting increase in unit discharge through the contraction, its impact may be less significant than that of other parameters such as flow velocity and sediment properties in many practical scenarios, since for the moderate contraction ratios present in the dataset the associated increase in shear stress is smaller than that produced by variations in the velocity ratio itself.

Table 3. RMSE values for different input combinations

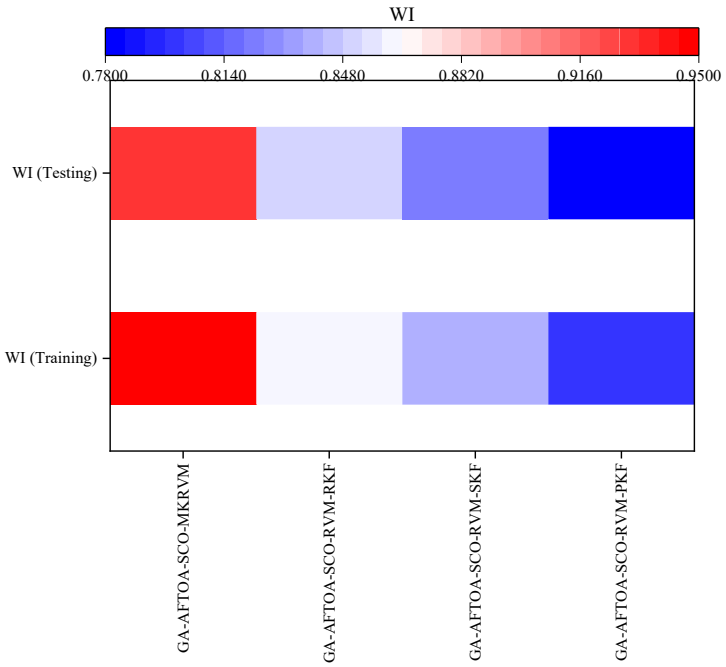
Input combination	RMSE
$ds = f(\frac{d_{50}}{h1}, \frac{u1}{uc}, \frac{b2}{b1})$	0.062
$\left(\frac{U_1}{U_c}, h_1, \frac{b_2}{b_1}\right)$	0.092
$\left(d_{50}, h_1, \frac{b_2}{b_1}\right)$	0.342
$\left(d_{50}, \frac{U_1}{U_c}, \frac{b_2}{b_1}\right)$	0.099
$\left(d_{50}, \frac{U_1}{U_c}, h_1\right)$	0.065

4.4 Investigation of the performance of the GA-AFTOA-SCO-MKRVM model for estimating scour depth

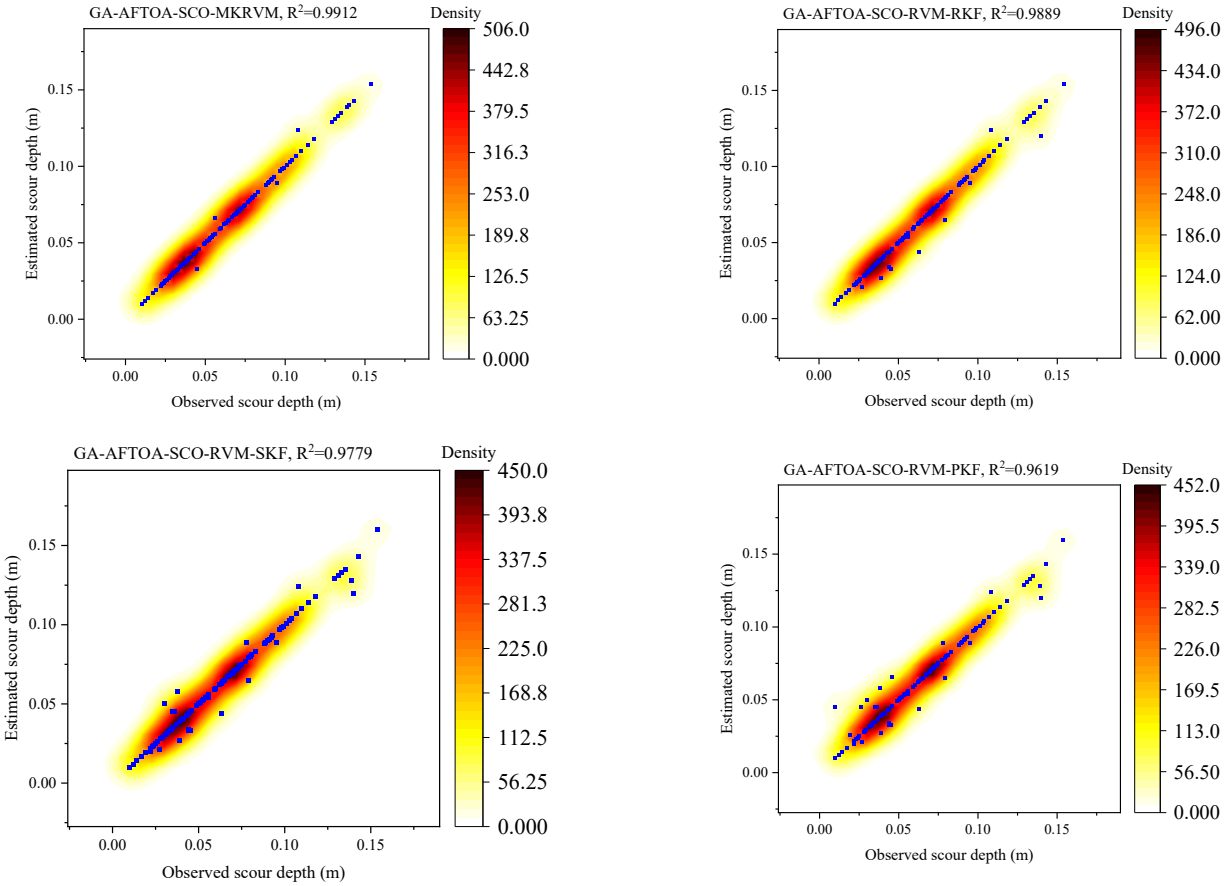
In this study, the GA-AFTOA-SCO-MKRVM model was used to estimate the scour depth. However, it is crucial to evaluate its capabilities compared to alternative models. This section compares the performance and robustness of the new model with three existing models: GA-AFTOA-SCO-RVM-PKF, GA-AFTOA-SCO-RVM-RKF, and GA-AFTOA-SCO-RVM-SKF. Figure 6a illustrates the WI values of the models at both the training and testing levels. The WI of the GA-AFTOA-SCO-MKRVM model was significantly better than that of the other models. Specifically, the new model enhanced the training and testing WI values of the other models by 9.4-15% and 8.6%-18%, respectively. These results highlighted the effectiveness of using a combination of kernel functions in machine learning models for estimating scour depth. By using multiple kernel functions, the new model was able to explore different aspects of the data space simultaneously, resulting in better performance and prediction accuracy. The results also revealed that the GA-AFTOA-RVM-PKF model had lower WI compared to other models. However, each of the kernel functions provides different advantages, which resulted in differences in the performance of estimation models.

Figure 6b shows scatterplots of heat, which depict the distribution of predicted data and the R^2 values of different models. It was observed that the GA-AFTOA-SCO-MKRVM model improved the R^2 values of other models by 1.1-3%. The main reasons for the good performance of the GA-AFTOA-SCO-MKRVM model were the proper adjustment of model parameters using a robust optimizer and the effectiveness of using a combination of kernel functions in analyzing data. The main reason for lower R^2 values of GA-AFTOA-SCO-RVM-SKF, GA-AFTOA-SCO-RVM-PKF, and GA-AFTOA-SCO-RVM-RKF models is that they fail to adequately capture the complexity and variability of the underlying data. Single kernel functions lack the flexibility to adapt to nonlinear relationships and patterns present in real-world datasets. As a result, they may oversimplify the data representation, which can result in lower accuracy of estimates, especially when dealing with complex or high-dimensional data.

The obtained results were also consistent with the studies conducted by Yu et al. and Abdelghafar et al. [18, 56] . These studies concluded that both the optimized RVM models and the MKRVM model outperformed the RVM model.



(a)



(b)

Figure 6. a: Heat map of WI for different predictive models and b: Heat scatterplots for the evaluation of the accuracy of the models

4.5 Evaluation of the accuracy of optimizers

In this study, multiple optimizers were utilized to adjust the model parameters. However, it is necessary to assess their performance in adjusting the model parameters. Figure 7 displays the PBIAS and MAE values of the different versions of MKRVM models developed using different optimizers. Since all of these models were built upon the MKRVM model as their foundation for estimating scour depth, comparing them can help determine which optimizer performs better in adjusting the parameters of the MKRVM model. This comparison allows the effectiveness of various optimization algorithms used for adjusting model parameters to be evaluated. Additionally, a trial-and-error method was also employed to adjust the parameters of the MKRVM model for comparison.

After analyzing the results, the performance of the proposed GA-AFTOA-SCO-MKRVM model was compared against two distinct sets of baseline models to evaluate its superiority. First, regarding the testing NSE, the proposed model demonstrated a significant improvement of 6.25%–31% when compared to the individual optimized MKRVM models (i.e., those tuned using PSO, FOA, GA, or AFTOA independently, without the full three-stage hybridization). Additionally, the model showed substantial enhancements in error metrics; the training and testing PBIASs were improved by 72%–93% and 32%–92%, respectively, relative to the individual optimized MKRVM models. Furthermore, when compared to the single-kernel RVM models (such as PKF, RKF, and SKF) optimized within the same framework, the proposed model exhibited further improvements in accuracy, specifically within the 8.6%–18% range.

The GA-AFTOA-SCO-MKRVM model achieved excellent performance by effectively combining the advantages of the three algorithms, resulting in improved convergence speed and higher-quality final solutions. Finally, it was observed that the standard MKRVM model exhibited the highest PBIAS and lowest NSE, which is attributed to the sub-optimal adjustment of its parameters.

The results of this section and the previous sections show that the new algorithm outperformed other optimizers in terms of both accuracy and convergence speed. Therefore, it is suitable for solving complex problems.

4.6 Comparison of the GA-AFTOA-SCO-MKRVM model with MLPs and RBFNNs

While the GA-AFTOA-SCO-MKRVM model proved to be reliable, it was necessary to further evaluate its performance to ensure its reliability. Therefore, it was compared with the GA-AFTOA-SCO-MLP and GA-AFTOA-SCO-RBFNN models. Figure 8 shows heatmaps that represent the MAE values for all three models. The GA-AFTOA-SCO-MKRVM model improved the training and testing MAEs of the other models by 33-48% and 23-51%, respectively. Thus, the GA-AFTOA-SCO-MKRVM model had the best performance. These findings underscore the effectiveness of the GA-AFTOA-SCO-MKRVM model in accurately estimating scour depth compared to alternative models. The improved performance of the GA-AFTOA-SCO-MKRVM model can be attributed to its ability to leverage multiple kernel functions for more comprehensive data representation.

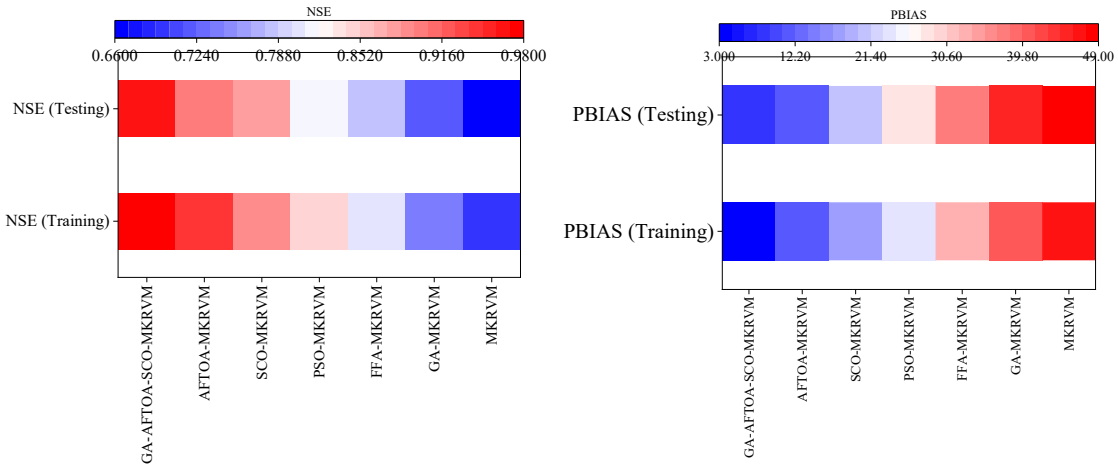


Figure 7. Heatmaps of PBIAS and NSE values of models for the evaluation of the performance of optimizers

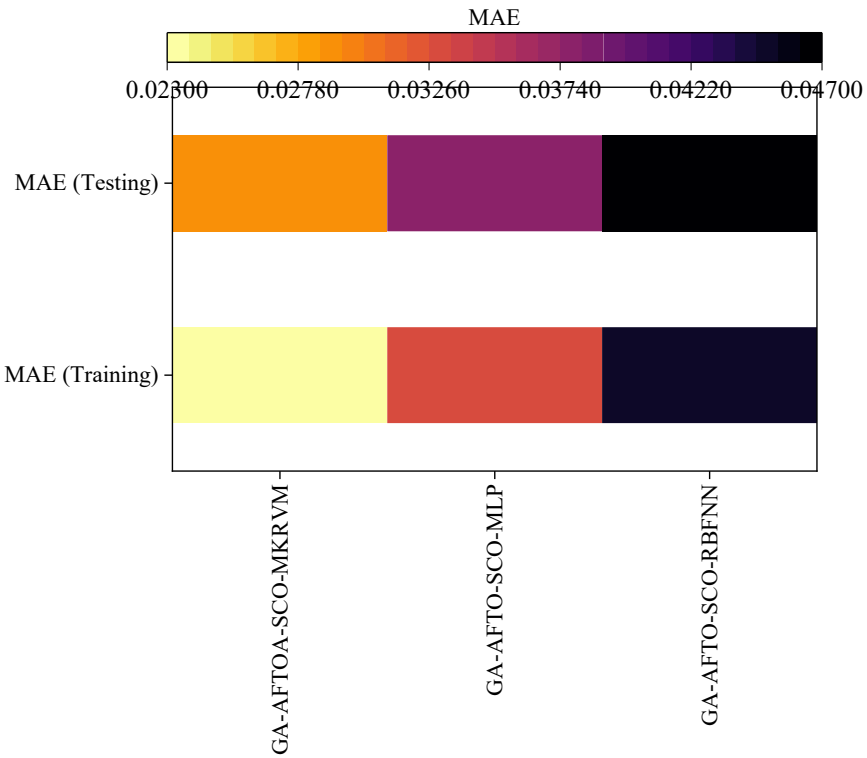


Figure 8. Comparison of the MAE of the GA-AFTO-SCO-MKRVM with that of other models

4.7 A Comparison between the GA-AFTOA-SCO-MKRVM model and empirical models

Researchers have developed various empirical models for estimating the scour depth. In this section, the performance of the new model is compared against these empirical models to demonstrate its effectiveness. The following empirical models were used for estimating the scour depth.

- Laursen [57]

$$\frac{d_s}{h_1} + 1 = \left(\frac{b_2}{b_1}\right)^{-0.75} \quad (28)$$

- Gill [52]

$$\frac{d_s}{h_1} + 1 = \left(\frac{b_2}{b_1}\right)^{-0.75} \quad (29)$$

- Lim [54]

$$\frac{d_s}{h_1} + 1 = 1.545 Fr_0{}^{0.75} \left(\frac{d_{50}}{h_1}\right)^{0.25} \left(\frac{b_2}{b_1}\right)^{-0.75} \quad (30)$$

$$Fr_0 = \frac{U_1}{\sqrt{g\left(\frac{\rho_s}{\rho_w}-1\right)}} \quad (31)$$

Where Fr_0 : Froude number, ρ_s : mass density of sediments. Figure 9 shows boxplots representing the statistical properties of the new model and the empirical models. The statistical characteristics of observed data were as follows: a median value of 0.063, a maximum value of 0.15, and a minimum value of 0.01. These statistical characteristics were completely consistent with those of the boxplot of the GA-AFTOA-SCO-MKRVM model. The boxplot of the GA-AFTOA-SCO-MKRVM model indicated a maximum value of 0.14, a minimum value of 0.01, and a median value of 0.063. On the other hand, the boxplots of the empirical models suggested that they did not accurately estimate the scour depth. For instance, the statistical characteristics of the Larsen model included a maximum of 0.18, a minimum of 0.01, and a median of 0.065. However, these statistical characteristics were not consistent with those observed in the data. It should be noted that these boxplot statistics (maximum, minimum, and median) summarize the overall distribution of the estimated values and can therefore be numerically close even between a well-performing and a poorly performing model, since they do not penalize point-by-point deviations between the estimated and observed scour depths for individual data points. Consequently, the boxplot comparison in this section should be interpreted as a check of overall distributional consistency, whereas the pointwise predictive accuracy of the models is more rigorously assessed by the RMSE, NSE, and WI values reported in Sections 4.4-4.6, which showed the GA-AFTOA-SCO-MKRVM model outperforming the other models by margins of 6.25-31%. The main reason for the poor performance of the empirical models was their reliance on simplified relationships and assumptions that did not fully capture the complexities of the scour process.

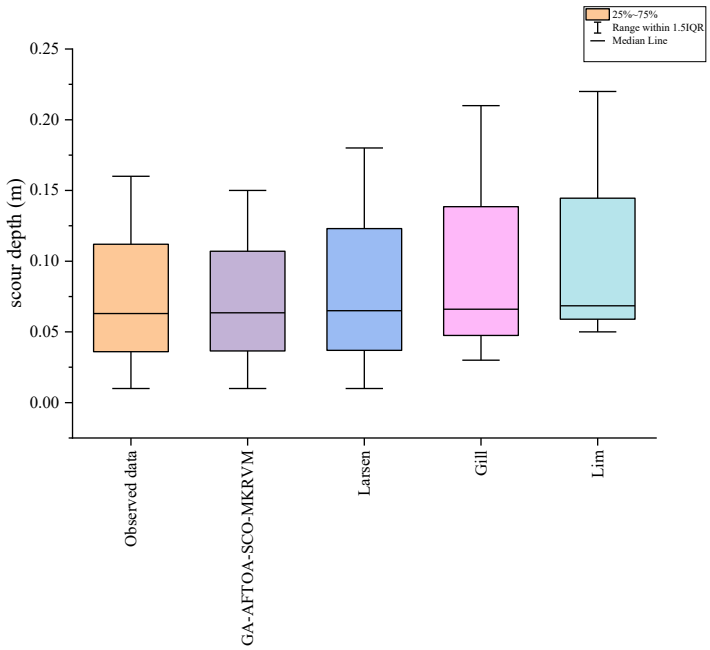


Figure 9. Boxplots of scour depth estimation models

4.8 A comparison between the current study and the previous study

While a comprehensive dataset was used to evaluate the performance of the new model in estimating scour depth, it was necessary to investigate its performance using an independent dataset. To accomplish this, an additional dataset that had been previously employed by Najafzadeh et al. [49] was used to estimate scour depth, and the accuracy of the models developed in this study was compared with that of their model. Both the 140-point dataset used in Section 3 and this 204-point dataset were compiled from the same set of long-contraction scour studies [50-54]; however, the 140-point dataset retains only the records for which the three non-dimensional groups used as inputs in the present study (d50/h1, u1/uc, and b2/b1, Equation 27) were fully and unambiguously reported, whereas the 204-point dataset of Najafzadeh et al. [49] also includes records described using their different combination of non-dimensional groups (below), so that the two datasets are overlapping but not identical subsets of the same source studies. They used $\frac{d_{50}}{b1}$, $\frac{h_1}{b1}$, $\frac{b_2}{b1}$, $\frac{U_1}{U_c}$, FR_0 (Froude number), and σ_g (geometric standard deviation) as input variables. All five of these input variables are non-dimensional groups derived through the same Buckingham Pi dimensional-analysis procedure as Equation 27, but following the specific grouping originally proposed and used by Najafzadeh et al. [49] for their ANFIS and SVM models; this combination, rather than the reduced three-parameter combination of Equation 27, was reproduced here so that the comparison against the ANFIS and SVM results reported in [49] would be made on a like-for-like basis. The number of data was 204. Table 4a shows details of the testing data. This data set was used to estimate scour depth and evaluate the performance of the new model. Table 4b shows the accuracy of different models. Najafzadeh et al. used the adaptive Neuro-fuzzy interface system (ANFIS) and the support vector machine (SVM) to estimate the scour depth. It was observed that the new model improved the R-value (correlation coefficient) of the ANFIS and SVM models by 6% and 5%, respectively [49]. Thus, the new model demonstrated a high ability to estimate scour depth based on various data sets.

Table 4. a: Details of the used data and b: R values of different models for estimating scour depth

a

Parameter	Value
$\frac{d_{50}}{b1}$	0.00875-0.2375
$\frac{h_1}{b1}$	0.0360-0.32
$\frac{b_2}{b1}$	0.33-4.062
$\frac{U_1}{U_c}$	0.432-1
FR_0	1.08-3.28

b

Model	R
ANFIS	0.88
SVM	0.89
GA-AFTO-SCO-MKRVM	0.94

4.9 Limitations and advantages of the new model in estimating scour depth

The previous sections show that the new model effectively estimates scour depth. However, it is important to note that this model has some limitations. The new model consists of four components, namely GA, AFTOA, SCO, and MKRVM, which may increase the training time. Figure 10 illustrates the training time of various models. It is evident that the new model requires more time for training compared to other models. Nevertheless, it is worth noting that there are advanced computer systems that can speed up the modeling process. In addition, the model was developed and validated using data from long channel contractions under clear-water flow conditions only, covering a limited range of sediment sizes, contraction ratios, and flume scales represented in the five source studies; consequently, its direct applicability to live-bed scour conditions, to other structure types such as bridge piers or abutments, or to prototype-scale contractions well outside the range of the laboratory data used here has not been established and would require further validation with independent data before field application.

Furthermore, it is important to acknowledge the inherent scale effects associated with laboratory flume data. The compiled dataset originates from physical models of varying scales, which may introduce discrepancies related to boundary friction and sediment cohesion compared to prototype-scale rivers. However, the source studies [50-54] strictly adhered to Froude similitude, and the sediment sizes (d50≥0.35 mm) were selected to eliminate cohesive forces. Moreover, the formulation of the model using dimensionless parameters (u1/uc, h1/d50, b2/b1) inherently normalizes the geometric and kinematic scales. Nevertheless, prior to field application, the model's predictions should be evaluated against prototype-scale data to account for any residual scale effects not captured in the laboratory environment.

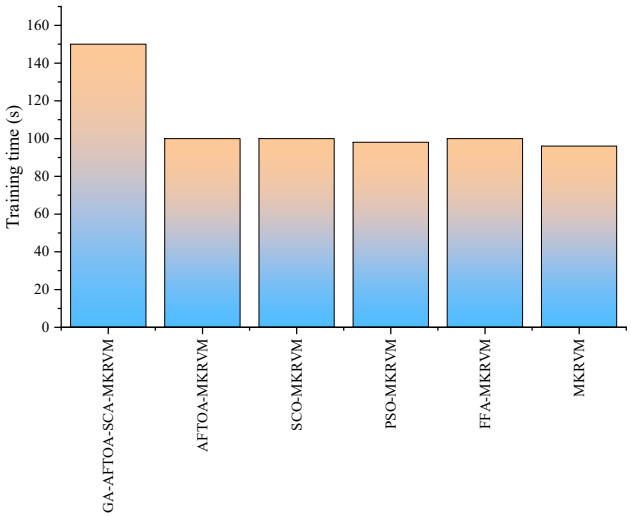


Figure 10. Training times of different models

However, the model developed in this study can be immensely useful for decision-makers in practical scenarios in several ways:

- Accurate Estimation: Decision-makers often need reliable estimates of scour depth to design and maintain hydraulic structures effectively. The GA-AFTOA-SCO-MKRVM model offers highly accurate estimations, empowering decision-makers to make informed choices regarding the design, maintenance, and management of these structures.
- Risk Assessment: Scour depth estimation is crucial for assessing the risk posed to hydraulic structures, such as bridges, dams, and pipelines. By accurately predicting scour depth, decision-makers can evaluate the safety and integrity of these structures and implement appropriate risk mitigation measures.
- Cost Reduction: Traditional methods of scour depth estimation may be time-consuming and costly. The GA-AFTOA-SCO-MKRVM model offers a more efficient and cost-effective alternative by providing accurate predictions with minimal resource expenditure, thereby reducing project costs.
- Optimized Resource Allocation: The new model provides precise estimates that help decision-makers effectively allocate resources for scour prevention and mitigation. By identifying high-risk areas and optimizing resource allocation, decision-makers can prioritize resources and achieve maximum impact in preventing and mitigating scour.
- Enhanced Infrastructure Resilience: By incorporating accurate scour depth estimates into infrastructure design and management practices, decision-makers can enhance the resilience of hydraulic structures against scour-related hazards, such as bridge collapse or pipeline failure, thereby ensuring the long-term sustainability of infrastructure systems.

5. Conclusion

Scour is a natural erosion process that occurs in riverbeds, near bridge piers, abutments, and other hydraulic structures. It can have various consequences for structures and ecosystems, which may vary based on the depth. Thus, accurate estimation of the scour depth is an important issue addressed in this article. In the first step, multiple kernel functions were incorporated into the RVM model to create a new version of this model called the MKRVM model. In the second step, a new hybrid optimizer called GA-AFTOA-SCO was created to adjust the parameters of the MKRVM model. Finally, a comprehensive dataset, including four input variables, was used to estimate the scour depth. The results showed that the GA-

AFTOA-SCO-MKRVM model demonstrated an improvement of 8.6-18% in testing the WI values compared to the other RVM models. In addition, the GA-AFTOA-SCO-MKRVM model showed a significant improvement of 6.25-31 % in the testing NSE compared to other optimized MKRVM models. The study also revealed several important findings. First, it demonstrated that the GA-AFTO-SCO algorithm achieved better accuracy and faster convergence compared to established algorithms. Second, it revealed that incorporating multiple kernel functions improved the performance of the RVM model in estimating the scour depth. However, there are still certain issues that can be addressed in future studies. First, it is important to quantify the uncertainties associated with the model parameters and inputs. Additionally, the new model can be utilized to estimate the score depth under complex conditions, such as live-bed scour and other structure geometries, provided it is retrained and validated on data representative of those conditions.

Funding Declaration

This work has been financially supported by the research deputy of Shahrekord University. The grant number was **96GRD1M44174.**

Conflict of interest

The authors state that they have no conflict of interest.

Not applicable.

Availability of data and materials

The datasets generated during and/or analyzed during the current study are available from the corresponding author on reasonable request.

Contribution

E.Gh: Writing, review, and code development, N.M: editing, developing codes, M.KH: Data analysis, editing and reviewing the manuscript.

Acknowledgement

The authors would like to sincerely thank Shahrekord University for providing the necessary facilities and environment to conduct this research.

References

1. Ghanbariadivi E, khosravi M. A comprehensive review of bridge pier scouring: Analysis of mechanisms and flow patterns, key factors, challenges, and protective measures. IWRJ. 2026;20(3):15-54. https://doi.org/10.22034/iwrj.2026.14891.2628
2. Alomari NK, Sihag P, Sami Al-Janabi AM, Yusuf B. Modeling of scour depth and length of a diversion channel flow system with soft computing techniques. Water Supply. 2023 Mar 1;23(3):1267-83.https://doi.org/10.2166/ws.2023.026
3. Choudhary A, Das BS, Devi K, Khuntia JR. ANFIS-and GEP-based model for prediction of scour depth around bridge pier in clear-water scouring and live-bed scouring conditions. Journal of Hydroinformatics. 2023 May 1;25(3):1004-28. https://doi.org/10.2166/hydro.2023.212
4. Kumar S, Goyal MK, Deshpande V, Agarwal M. Estimation of time dependent scour depth around circular bridge piers: Application of ensemble machine learning methods. Ocean Engineering. 2023 Feb 15;270:113611. https://doi.org/10.1016/j.oceaneng.2022.113611
5. Jalil-Masir, H., Fattahi, R., Ghanbari-Adivi, E. and Aghbolaghi, M.A., 2021. Effects of different forest cover configurations on reducing the solitary wave-induced total sediment transport in coastal areas: An experimental study. Ocean Engineering, 235, p.109350. 10.1016/j.oceaneng.2021.109350
6. Mirzaee R, Mohammadi M, Mousavi SF, Bagherzadeh M, Hosseini K. Application of soft computing techniques to estimate the scouring depth formed by crossing jets. Water Science & Technology. 2023 Apr 15;87(8):1853-65. https://doi.org/10.2166/wst.2023.108
7. Nezaratian H, Hassanjabbar A, Wu P. Estimation of maximum scour depth around bridge piers under ice-covered conditions using data-driven methods. International Journal of Sediment Research. 2023 Apr 1;38(2):191-202. https://doi.org/10.1016/j.ijsrc.2022.07.008
8. Kumar L, Afzal MS. Estimating pier scour depth under combined waves and current using boosting machine-learning models.

Acta Geophysica. 2024 Jun;72(3):1895-911. https://doi.org/10.1007/s11600-023-01089-2
9. Devi G, Kumar M. Last century evolution in local scour measuring techniques. InCurrent Directions in Water Scarcity Research 2022 Jan 1 (Vol. 7, pp. 513-529). Elsevier. 10.1016/B978-0-323-91910-4.00029-7
10. San Martin C, Rifo C, Guerra M, Ettmer B, Link O. Monitoring scour at bridge piers in rivers with supercritical flows. Hydrology. 2023 Jul 13;10(7):147. https://doi.org/10.3390/hydrology10070147
11. Deng Z, Huang M, Wan N, Zhang J. The current development of structural health monitoring for bridges: A review. Buildings. 2023 May 23;13(6):1360. https://doi.org/10.3390/buildings13061360
12. Pandey M, Karbasi M, Jamei M, Malik A, Pu JH. A Comprehensive Experimental and Computational Investigation on Estimation of Scour Depth at Bridge Abutment: Emerging Ensemble Intelligent Systems: M. Pandey et al. Water Resources Management. 2023 Jul;37(9):3745-67. https://doi.org/10.1007/s11269-023-03525-w
13. Behera P, Padhi E, Pal M. Hybrid machine learning and metaheuristic optimization approach for accurate prediction of pier scour depth under clear-water and live-bed scour condition. Expert Systems with Applications. 2026 Jul 15;320:132217. https://doi.org/10.1016/j.eswa.2026.132217
14. Kanishkavardhan P, Maheswari N, Nithilan B, Mohamed Aman A. Scour depth prediction using machine learning and explainable AI: assessment of bridge vulnerability. Frontiers in Built Environment. 2026;12:1790274. https://doi.org/10.3389/fbuil.2026.1790274
15. Adnan RM, Mostafa RR, Dai HL, Heddam S, Kuriqi A, Kisi O. Pan evaporation estimation by relevance vector machine tuned with new metaheuristic algorithms using limited climatic data. Engineering Applications of Computational Fluid Mechanics. 2023 Dec 31;17(1):2192258. https://doi.org/10.1080/19942060.2023.2192258
16. Adnan RM, Mostafa RR, Dai HL, Heddam S, Kuriqi A, Kisi O. Pan evaporation estimation by relevance vector machine tuned with new metaheuristic algorithms using limited climatic data. Engineering Applications of Computational Fluid Mechanics. 2023 Dec 31;17(1):2192258. https://doi.org/10.1002/for.3028
17. Jabbari MR, Dorafshan MM, Eslamian S. Relevance vector machine (RVM). InHandbook of Hydroinformatics 2023 Jan 1 (pp. 365-384). Elsevier. 10.1016/B978-0-12-821285-1.00008-7
18. Yu X, Li J, Kang F. A hybrid model of bald eagle search and relevance vector machine for dam safety monitoring using long-term temperature. Advanced Engineering Informatics. 2023 Jan 1;55:101863. 10.1016/j.aei.2022.101863
19. Xie B, Peng C, Wang Y. Combined relevance vector machine technique and subset simulation importance sampling for structural reliability. Applied Mathematical Modelling. 2023 Jan 1;113:129-43. https://doi.org/10.1016/j.apm.2022.09.010
20. Saeid F, Irandoust M, Jalalkamali N. Development of soft computing models based on wavelet analysis for estimating piezometric heads in earth dams. Iranian Journal of Science and Technology, Transactions of Civil Engineering. 2023 Dec;47(6):3731-42. https://doi.org/10.1007/s40996-023-01164-0
21. Yaseen ZM, Mohtar WH, Homod RZ, Alawi OA, Abba SI, Oudah AY, Togun H, Goliatt L, Kazmi SS, Tao H. Heavy metals prediction in coastal marine sediments using hybridized machine learning models with metaheuristic optimization algorithm. Chemosphere. 2024 Mar 1;352:141329. https://www.sciencedirect.com/science/article/pii/S0951832023008049
22. Bouchehed A, Laouacheria F, Heddam S, Djemili L. Machine learning for better prediction of seepage flow through embankment dams: Gaussian process regression versus SVR and RVM. Environmental Science and Pollution Research. 2023 Feb;30(9):24751-63. https://doi.org/10.1007/s11356-023-25446-2
23. Chen F, Cheng M, Tang B, Xiao W, Chen B, Shi X. A novel optimized multi-kernel relevance vector machine with selected sensitive features and its application in early fault diagnosis for rolling bearings. Measurement. 2020 May 1;156:107583. https://doi.org/10.1016/j.measurement.2020.107583
24. Chen F, Yang Y, Tang B, Chen B, Xiao W, Zhong X. Performance degradation prediction of mechanical equipment based on optimized multi-kernel relevant vector machine and fuzzy information granulation. Measurement. 2020 Feb 1;151:107116.

https://doi.org/10.1016/j.measurement.2019.107116
25. Chen S, Gu C, Lin C, Zhang K, Zhu Y. Multi-kernel optimized relevance vector machine for probabilistic prediction of concrete dam displacement. Engineering with Computers. 2021 Jul;37(3):1943-59. https://doi.org/10.1007/s00366-019-00924-9
26. Sadeghfam S, Daneshfaraz R, Khatibi R, Minaei O. Experimental studies on scour of supercritical flow jets in upstream of screens and modelling scouring dimensions using artificial intelligence to combine multiple models (AIMM). Journal of Hydroinformatics. 2019 Sep 1;21(5):893-907. https://doi.org/10.2166/hydro.2019.076
27. Daneshfaraz R, Abam M, Heidarpour M, Abbasi S, Seifollahi M, Abraham J. The impact of cables on local scouring of bridge piers using experimental study and ANN, ANFIS algorithms. Water Supply. 2022 Jan 1;22(1):1075-93. https://doi.org/10.2166/ws.2021.215
28. Wang Y, Xie B. Adaptive relevance vector machine combined with Markov-chain-based importance sampling for reliability analysis. Reliability Engineering & System Safety. 2022 Apr 1;220:108287. 10.1016/j.ress.2021.108287
29. Qiu JS, Fan YC, Wang SL, Yang X, Qiao JL, Liu DL. Research on the remaining useful life prediction method of lithium-ion batteries based on aging feature extraction and multi-kernel relevance vector machine optimization model. International Journal of Energy Research. 2022 Aug;46(10):13931-46. https://doi.org/10.1002/er.8110
30. Braik M. Enhanced ali baba and the forty thieves algorithm for feature selection. Neural Computing and Applications. 2023 Mar;35(8):6153-84. https://doi.org/10.1007/s00521-022-08015-5
31. Alphonse AS, Abinaya S, Abirami S. Alibaba and forty thieves algorithm and novel prioritized Prewitt pattern (PPP)-based convolutional neural network (CNN) using hyperspherically compressed weights for facial emotion recognition. Journal of Visual Communication and Image Representation. 2023 Dec 1;97:103948. https://doi.org/10.1016/j.jvcir.2023.103948
32. Mahdad B. Optimal power management of DGS and DSTATCOM using improved Ali Baba and the forty thieves optimizer. Facta Universitatis, Series: Electronics and Energetics. 2023 Mar 20;36(1):053-75. https://doi.org/10.2298/fuee2301053m
33. Alweshah M, Almiani M, Alkhalaileh S, Kassaymeh S, Hezzam EA, Alomoush W. Parallel metaheuristic algorithms for solving imbalanced data classification problems. IEEE Access. 2023 Oct 12;11:114443-58. https://doi.org/10.1109/ACCESS.2023.3324061
34. Papazoglou G, Biskas P. Review and comparison of genetic algorithm and particle swarm optimization in the optimal power flow problem. Energies. 2023 Jan 20;16(3):1152. https://doi.org/10.3390/en16031152
35. Sohail A. Genetic algorithms in the fields of artificial intelligence and data sciences. Annals of Data Science. 2023 Aug;10(4):1007-18. https://doi.org/10.1007/s40745-021-00354-9
36. Cavallaro C, Cutello V, Pavone M, Zito F. Machine Learning and Genetic Algorithms: A case study on image reconstruction. Knowledge-Based Systems. 2024 Jan 25;284:111194. https://doi.org/10.1016/j.knosys.2023.111194
37. Attouri K, Dhibi K, Mansouri M, Hajji M, Bouzrara K, Nounou H. Enhanced fault diagnosis of wind energy conversion systems using ensemble learning based on sine cosine algorithm. Journal of Engineering and Applied Science. 2023 Dec;70(1):56. https://doi.org/10.1186/s44147-023-00227-3
38. Zhong M, Wen J, Ma J, Cui H, Zhang Q, Parizi MK. A hierarchical multi-leadership sine cosine algorithm to dissolving global optimization and data classification: The COVID-19 case study. Computers in Biology and Medicine. 2023 Sep 1;164:107212. https://doi.org/10.1016/j.compbiomed.2023.107212
39. Santhiya C, Padmavathi S. Bio-Inspired crossover cosine swarm optimization algorithm based task scheduling for quality of service improvement under cloud environment. Journal of Signal Processing Systems. 2024 Jan;96(1):51-65. https://doi.org/10.1007/s11265-023-01900-9
40. Alhijawi B, Awajan A. Genetic algorithms: Theory, genetic operators, solutions, and applications. Evolutionary intelligence. 2024 Jun;17(3):1245-56. https://doi.org/10.1007/s12065-023-00822-6
41. Sejuti ZA, Islam MS. A hybrid CNN–KNN approach for identification of COVID-19

with 5-fold cross validation. Sensors International. 2023 Jan 1;4:100229. https://doi.org/10.1016/j.sintl.2023.100229
42. Afzal S, Ziapour BM, Shokri A, Shakibi H, Sobhani B. Building energy consumption prediction using multilayer perceptron neural network-assisted models; comparison of different optimization algorithms. Energy. 2023 Nov 1;282:128446. https://doi.org/10.1016/j.energy.2023.128446
43. Ghimire S, Nguyen-Huy T, Prasad R, Deo RC, Casillas-Perez D, Salcedo-Sanz S, Bhandari B. Hybrid convolutional neural network-multilayer perceptron model for solar radiation prediction. Cognitive Computation. 2023 Mar;15(2):645-71. https://doi.org/10.1007/s12559-022-10070-y
44. Wu J, Fang L, Dong G, Lin M. State of health estimation of lithium-ion battery with improved radial basis function neural network. Energy. 2023 Jan 1;262:125380. https://doi.org/10.1016/j.energy.2022.125380
45. Heidari A, Navimipour NJ, Unal M. A secure intrusion detection platform using blockchain and radial basis function neural networks for internet of drones. IEEE Internet of Things Journal. 2023 Jan 20;10(10):8445-54. https://doi.org/10.1109/JIOT.2023.3237661
46. Kashani AR, Chiong R, Mirjalili S, Gandomi AH. Particle Swarm Optimization Variants for Solving Geotechnical Problems: Review and Comparative Analysis: AR Kashani et al. Archives of Computational Methods in Engineering. 2021 May;28(3):1871-927. https://doi.org/10.1007/s11831-020-09442-0
47. Sharafi M, Samadianfard S, Behmanesh J, Prasad R. Integration of fruit fly and firefly optimization algorithm with support vector regression in estimating daily pan evaporation. International Journal of Biometeorology. 2024 Feb;68(2):237-51… https://doi.org/10.1007/s00484-023-02586-1
48. Zhang L. A tree-based energy-aware data aggregation method in the Internet of Things using the firefly optimization algorithm. Multiscale and Multidisciplinary Modeling, Experiments and Design. 2023 Jun;6(2):223-33. https://doi.org/10.1007/s41939-023-00141-4
49. Najafzadeh M, Etemad-Shahidi A, Lim SY. Scour prediction in long contractions using ANFIS and SVM. Ocean Engineering. 2016 Jan 1;111:128-35. 10.1016/j.oceaneng.2015.10.053
50. Dey S, Raikar RV. Scour in long contractions. Journal of Hydraulic Engineering. 2005 Dec;131(12):1036-49. https://doi.org/10.1061/(asce)0733-9429(2005)131:12(1036)
51. Komura S. Equilibrium depth of scour in long constrictions. Journal of the Hydraulics Division. 1966 Sep;92(5):17-37. https://doi.org/10.1061/JYCEAJ.0001504
52. Gill MA. Bed erosion in rectangular long contraction. Journal of the Hydraulics Division. 1981 Mar;107(3):273-84. https://doi.org/10.1061/jyceaj.0005626
53. Webby MG. General scour at contraction. RRU bulletin. 1984;73:109-18. https://www.researchgate.net/publication/291191849_General_scour_at_a_contraction#fullTextFileContent
54. Slow Yong Lim, Lim S. Clear water scour in long contractions. Proceedings of the Institution of Civil Engineers-Water Maritime and Energy. 1993 Jun 1;101(2):93-8. https://doi.org/10.1680/iwtme.1993.23590
55. Nti IK, Nyarko-Boateng O, Aning J. Performance of machine learning algorithms with different K values in K-fold cross-validation. International Journal of Information Technology and Computer Science. 2021;13(6):61-71. https://doi.org/10.5815/ijitcs.2021.06.05
56. Abdelghafar S, Farrag TA, Zanaty A, Alshater H, Darwish A, Hassanien AE. Pattern and predictors of death from aluminum and zinc phosphide poisoning using multi-kernel optimized relevance vector machine. Scientific Reports. 2023 May 22;13(1):8268. https://doi.org/10.1038/s41598-023-34489-x
57. Laursen EM. An analysis of relief bridge scour. Journal of the Hydraulics Division. 1963 May;89(3):93-118. https://doi.org/10.1061/JYCEAJ.000089

© 2027 by the authors. Licensee SCU, Ahvaz, Iran. This article is an open access article distributed under the terms and conditions of the Creative Commons Attribution 4.0 International (CC BY 4.0 license) (http://creativecommons.org/licenses/by/4.0/).